Nano Research

Open Access

Research Article

Construction of Ni single-atom coordinated with doped N and S elements for mild hydrogenation of methyl acrylate to methyl propionate

Taolue Sun[1,3], Chen Jian[1], Gang Wang[1], Hui Zhao[1], Guoliang Zhang[1,3,4], Zengxi Li[1,2] ✉, and Chunshan Li[1,3] ✉

[1] *State Key Laboratory of Mesoscience and Engineering, CAS Key Laboratory of Green Process and Engineering, Beijing Key Laboratory of Ionic Liquids Clean Process, Institute of Process Engineering, Chinese Academy of Sciences, Beijing 100190, China*
[2] *School of Chemical Engineering, University of Chinese Academy of Sciences, Beijing 100049, China*
[3] *Huizhou Institute of Green Energy and Advanced Materials, Huizhou 516081, China*
[4] *Advanced Energy Science and Technology Guangdong Laboratory, Huizhou 516081, China*

Cite this article: *Nano Research*, **2025**, *18*, 94907053. https://doi.org/10.26599/NR.2025.94907053

ABSTRACT: Although the nickel-based catalyst is able to exhibit comparative catalytic activity to noble metal for methyl acrylate hydrogenation, it requires strict reaction condition, which can be improved by regulation of coordination environment. In this study, we constructed a kind of Ni single-atom coordinated with N and S (Ni-NSC) through the pyrolysis of organic Ni-based precursors at 600 °C. The existence and fine structure of Ni single-atom were confirmed by the spherical electron microscopic observation in combination with the X-ray absorption spectroscopy (XAS) characterization. In addition, the catalytic hydrogenation assessment suggested that the as-prepared Ni-NSC catalyst exhibited higher activity and stability than the Ni/NSC supported catalyst prepared by incipient wetness impregnation method. This remarkable catalytic activity was due to the high dispersion and density of Ni single-atom and weak adsorption energy of intermediates on these Ni sites.

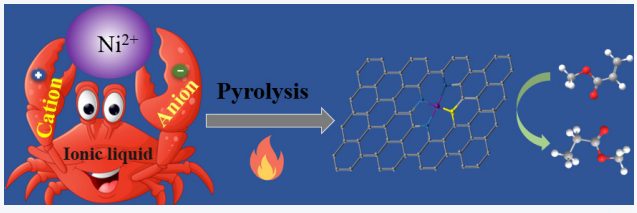

KEYWORDS: methyl acrylate, mild hydrogenation, Ni single-atom, coordination environment, adsorption energy

1 Introduction

As an important chemical raw material and intermediate, methyl propionate (MP) is commonly utilized as a solvent for cellulose nitrate, paint, spices, and condiments [1–4]. The preparation of MP form methyl acrylate (MA) by hydrogenation has been widely concerned for its efficient atomic utilization and green generation process. Considering the easy polymerization of MA at relative temperature, the reported catalysts are primarily noble metals (Pd, Au, and Rh), which show excellent catalytic activity under mild reaction condition [5–7]. However, the disadvantages like high cost, easy inactivation, and limited storage of these noble meals also restrict their industrial application. Therefore, the development of non-noble mental catalyst with highly catalytic efficiency at mild condition is desired.

The noble-metal catalysts are frequently utilized in the hydrogenation reaction attributing to their higher catalytic activity under mild reaction condition. Yukihide Shiraishi reported a kind of platinum nanoclusters and evaluated the catalytic activity in the hydrogenation of MA under atmospheric pressure at 30 °C. The experimental results demonstrated that the effectiveness of the catalyst was influenced by the size of the metal nanoclusters [8]. Toru Matsushita synthesized the Pd/Ag/Rh trimetallic catalyst, and the relationship between the catalytic activity and average particle size of trimetallic, bimetallic, and monomerallic nanoparticles was also studied. The results revealed that the catalytic performance on hydrogenation was improved with the decrease in particle size of active component [9]. M. van der Zon compared the catalytic activity of Pd/C and Pd/Al_2O_3 in the hydrogenation of MA, and the transmission electron microscopy (TEM) characterization results showed that the dispersion of catalyst particles had a great influence on the catalytic activity, and the agglomeration of active components would lead to the decrease of hydrogenation performance [10]. Chen synthesized the Pd-based catalyst with relatively high dispersion using polyfunctional phosphin ligands and obtained 100% yield of MP from the hydrogenation of MA [11]. Recently, the Ni-based catalysts have received more and more attention because of their low preparation cost and comparable

Received: June 28, 2024; **Revised:** September 25, 2024
Accepted: September 26, 2024

✉Address correspondence to Zengxi Li, zxli@home.ipe.ac.cn; Chunshan Li, csli@ipe.ac.cn

hydrogenation activity to noble metal, especially for the Pd catalysts. In addition, the nickel element is also one of the most suitable active components for C=C hydrogenation.

In last decades, great efforts have been made to promote the catalytic performance of non-noble metal catalysts, such as doping additives and improving preparation methods [12, 13]. It has been demonstrated that the dispersion and particle size of metal nanoclusters are close to the reactivity of catalysts with metal nanocluster. However, most of the non-noble metal catalysts require harsh reaction conditions, like higher reaction temperature and pressure. Recently, the single-atom catalyst (SAC) has caused extensive interest of researchers, due to the utilization of maximum atomic sites and strong metal–substrate interactions of active component. At present, the saturated M-N_4 coordination is the most stable structure of single-atom catalyst, among which the Ni-SACs present relatively high hydrogenation efficiency in the current research. Liu synthesized a type of Ni-SACs with Ni-N_4 structure using Ni(phen)$_3$ complex as precursor, which showed high activity and ultrastability in cellulose hydrolysis [14]. Dai also developed the Ni-N-C single-atom catalyst by pyrolysis of ZnNi-ZIF (ZIF = zeolitic imidazolate framework) precursor at high temperature, which exhibited high activity in acetylene hydrogenation [15]. Recently, it was discovered that the unsaturated Ni-N_x with low coordination number has higher catalytic activity [16–18], which was usually prepared by the replacement of N atom with heteroatom of P or S [19, 20]. Compared with the N atom, the heteroatom has relatively large atomic radius and is easy to generate defects on the carbon materials. Meanwhile, the lower electronegativity of heteroatom can regulate the electronic structure of Ni-N_4 active site. Qu prepared the Ni-P_1N_3 catalyst with Ni single sites for CO_2 reduction, which showed higher activity than Ni-N_4 catalyst [21]. However, the specific regulatory mechanism of heteroatom on the catalytic performance of SACs is still unclear. Therefore, it is necessary to study the promotional effect of heteroatom doping on catalytic performance systematically.

In this study, a green and environmentally friendly method for the doping of S and N atoms onto Ni-C was rationally designed by pyrolysis of ionic liquid precursor containing S and N elements. Atomically dispersed metal atoms provide more active sites, which makes the catalyst show better hydrogenation activity. Furthermore, the related coordination number and environment of active Ni sites were investigated employing X-ray absorption spectroscopy (XAS) characterization. The existence of Ni single-atom was confirmed by spherical electron microscopic observation. The promotional effect of specific Ni-carbon materials with N and S doping (NSC) structure on the catalytic hydrogenation performance was illustrated by comparison with the Ni/NSC supported catalyst through catalytic assessment in combination with density functional theory (DFT) calculations.

2 Experimental

2.1 Main materials

MA (purity ≥ 99.0%) was provided by Damao Chemical Reagent Factory (Tianjin, China). Absolute ethyl alcohol (purity ≥ 99.7%) was purchased from Beijing Tongguang Fine Chemical Co., Ltd. (Beijing, China). Nickel acetate ($NiC_4H_6O_4{\cdot}4H_2O$, purity ≥ 99.0%) and magnesium oxide (MgO) were obtained from Macklin Biochemical Co., Ltd. (Shanghai, China). 1-butyl-3-methyl-imidazolium-tosylate (purity ≥ 97%) was provided by Beijing Wokai Biotechnology Co., Ltd. (Beijing, China). Hydrochloric acid (HCl, 36 wt.%–38 wt.%) was acquired from Xilong Co., Ltd. (Guangdong, China).

2.2 Catalyst preparation

To prepare Ni-NSC catalyst, the mixture of 1-butyl-3-methyl-imidazolium-tosylate (0.47 g) and $NiC_4H_6O_4{\cdot}4H_2O$ (0.12 g) was first added to absolute ethyl alcohol and stirred for 10 min, and then MgO (2 g) was added to the above mixture. The mixture was stirred at 60 °C under refluxing for 12 h. The absolute ethyl alcohol was removed by rotary evaporation at 60 °C, and the obtained solids were dried under vacuum at 60 °C for 12 h. Then, the solids were transferred to a quartz boat and pyrolyzed under NH_3 atmosphere at 600 °C for 2 h with a ramp of 2 °C·min^{-1}. The catalyst precursors were treated by 1 M HCl to remove MgO and Ni nanoparticles, and then the products were dried under vacuum at 60 °C for 12 h. Before test, the Ni-NSC catalyst was activated by 10% H_2/N_2 at 450 °C for 4 h. Samples pyrolyzed at different temperatures were denoted as Ni-NSC-T (T = pyrolysis temperature). In the same procedure, the NSC support was also prepared without the addition of $NiC_4H_6O_4{\cdot}4H_2O$. For comparison, the Ni/NSC catalyst was prepared by wetness impregnation method. First, 300 mg NSC support was impregnated in ethanol solution (3 g) containing 13.5 mg $NiC_4H_6O_4{\cdot}4H_2O$. Then the obtained sample was aged at room temperature for 12 h, followed by dryness at 120 °C for 12 h and calcination at 450 °C for 4 h in NH_3 atmosphere.

2.3 Material characterization

X-ray diffraction (XRD) patterns were recorded on a Rigaku Smart Lab X-ray powder diffractometer using Cu Kα radiation in the range of $5° < 2\theta < 90°$. Raman spectra were taken on Via Raman microscope in the range of 500–2600 cm^{-1}. N_2 adsorption–desorption isotherms were obtained to observe the surface area and the pore size on a micromeritics ASAP 2460 apparatus. The Ni metal loadings of the catalysts were analyzed by inductively coupled plasma-optical emission spectroscopy (ICP-OES) on a PerkinElmer Optima 8000 instrument. The contents of N and S in the catalysts were tested by CHNS elemental analyzer on a Vario MACRO cube instrument. High resolution TEM (HRTEM) examinations were carried out in a FEI Talos F2000x instrument. The high-angle annular dark-field scanning transmission electron microscopy (HAADF-STEM) images were obtained by JEOLM-ARM300F at an accelerating voltage of 300 kV. Before the observation, the catalyst powder was grounded to 200 meshes. X-ray photoelectron spectroscopy (XPS) analysis was obtained on a Thermo Scientific K-Alpha electron spectrometer with Al Kα as the excitation source, operated at 12 kV and 6 mA. All of the binding energies of the catalysts were corrected with C 1s (284.8 eV) as the reference. The Ni K-edge X-ray absorption fine structure (XAFS) spectra were collected at the XAFS station of the BL14B2 beamline in Super Photon ring-8 (SPring-8).

2.4 Catalyst activity measurements

All the catalysts were evaluated via the hydrogenation of MA in a 100 mL stainless-steel autoclave at 70 °C and H_2 pressure of 1 MPa. Before the hydrogenation experiment, the catalyst samples (50 mg) were reduced in 10% H_2 at 450 °C for 4 h. After that, the catalysts (50 mg), MA (250 mg), and anhydrous ethanol (20 mL) were

charged in the batch reactor. The temperature was raised to 70 °C under stirring speed of 600 r·min^{-1}. After the completion of reaction, the products were filtered by filtration membrane and analyzed on gas chromatography (SP-7890). The stability of Ni-NSC-600 and Ni/NSC catalyst was studied by cyclic experiments. After the hydrogenation reaction, the solid catalyst was recovered by filtering the reaction mixture and washed with ethanol for three times, then the catalyst was dried at 120 °C for 8 h to prepare for the next hydrogenation experiment.

3 Results and discussion

3.1 Characterization of physicochemical properties

Figure 1(a) illustrates the synthesis of Ni-NSC catalyst. A complex precursor of 1-butyl-3-methyl-imidazolium-tosylate and $NiC_4H_6O_4{\cdot}4H_2O$ was dispersed on the surface of MgO, then the mixture was pyrolyzed at 500–700 °C in NH_3 atmosphere for 2 h. After that, the obtained powder was etched with 1 M HCl. Figure 1(b) shows the Raman spectra of catalysts prepared at different pyrolysis temperatures. The D band peaks around 1580 cm^{-1} are associated with the disorders and defects of the carbon structure. While the G band peaks around 1350 cm^{-1} are attributed to the vibration of sp^2 carbon [22, 23]. It can be found that the I_D/I_G increases gradually with the elevation of pyrolysis temperature, suggesting that the carbon materials have more defects and disorders, which facilitates the generation of more active sites. Besides, no other peak is found in the Raman spectra. However, it can be seen from the XRD patterns of the Ni-NSC catalysts obtained at different pyrolysis temperatures, as shown in Fig. 1(c), that new diffraction of NiO is observed at 700 °C, indicating that the higher temperature leads to the agglomeration of Ni atoms. ICP analysis results (Table S1 in the Electronic Supplementary Material (ESM)) demonstrated that the Ni loading gradually increases when the pyrolysis temperature is increased to 600 °C (1.33 wt.%), and then it decreases with the temperature being further enhanced to 700 °C. In addition, no other Ni diffraction peak is found in both Raman and XRD spectra of Ni-NSC-600, indicating that the Ni species show good dispersion on the catalyst. For Ni/NSC catalyst, as shown in Fig. S1 in the ESM, there is obvious agglomeration phenomenon.

The Brunauer–Emmett–Teller (BET) surface area, which also has a great influence on the dispersion of Ni species, was obtained and the results are shown in Fig. S2 in the ESM. The catalyst had a significantly larger BET surface area (793 m^2·g^{-1}) at 600 °C, and then it decreased gradually with the increase of pyrolysis temperature, which may be due to the collapse of the material under high temperature. There are no obvious nickel particles in HRTEM image, as shown in Fig. 1(d). So, the aberration-corrected HAADF-STEM was utilized to confirm the invisible Ni particles in the Ni-NSC-600 catalyst, as presented in Fig. 1(e). Considerable number of bright spots are noticed on the carbon surface, indicating that the Ni element is atomically dispersed on the carbon support. Furthermore, the energy dispersive X-ray spectroscopy (EDS) elemental mapping images (Fig. 1(f)) show that the Ni element is uniformly distributed throughout the entire nanostructure without obvious agglomeration phenomenon. In addition, the N and S elements are also found to be uniformly distributed on the catalyst, revealing that the catalyst was simultaneously doped with N and S components.

The catalysts were further analyzed by XPS characterization to investigate the Ni chemical state, and their deconvolution and related parameters are shown in Fig. 2 and Table S2 in the ESM. Figure 2(a) shows the full XPS spectrum of Ni-NSC-600 catalyst, and the Mg signal is not noticed, indicating that the MgO has been completely removed in the pickling process. Figure 2(b) shows the Ni 2p XPS spectra of Ni-NSC-600 and Ni/C catalysts, and the binding energy of Ni $2p_{3/2}$ in Ni-NSC-600 is lower than that

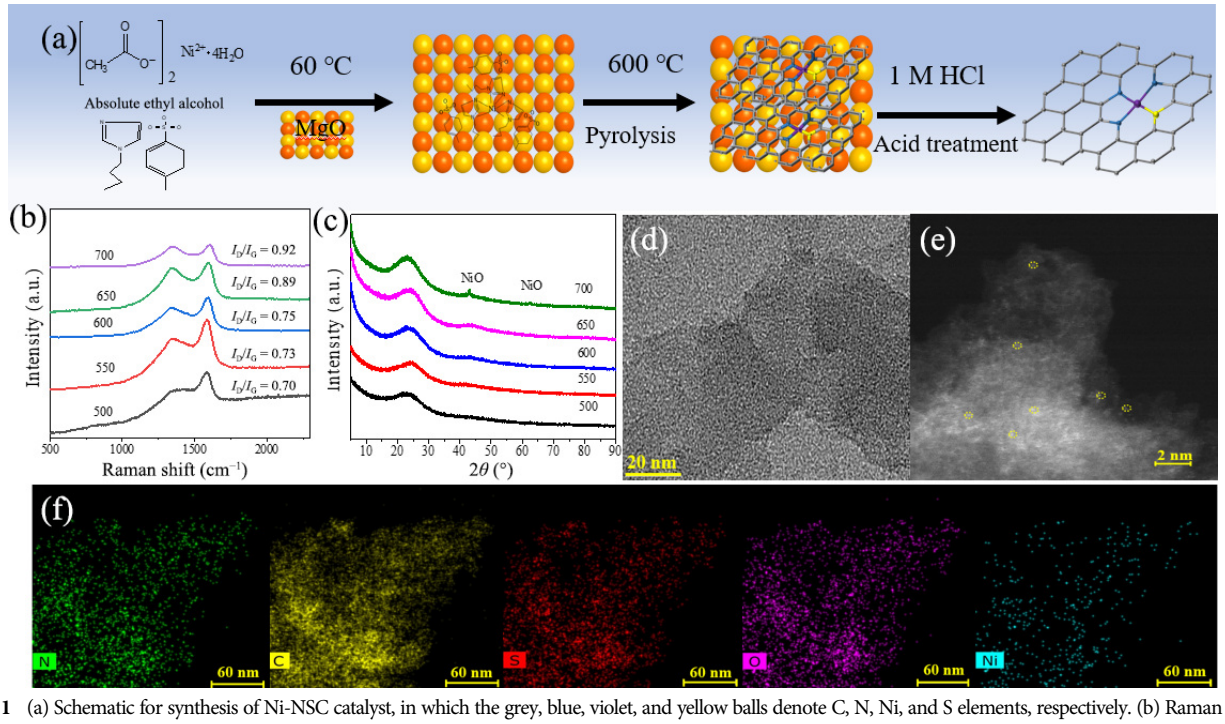

Figure 1 (a) Schematic for synthesis of Ni-NSC catalyst, in which the grey, blue, violet, and yellow balls denote C, N, Ni, and S elements, respectively. (b) Raman spectra and (c) XRD patterns of Ni-NSC catalyst series prepared at different pyrolysis temperature. (d) HRTEM, (e)HAADF-STEM, and (f) EDS elemental mapping images of Ni-NSC-600 catalyst.

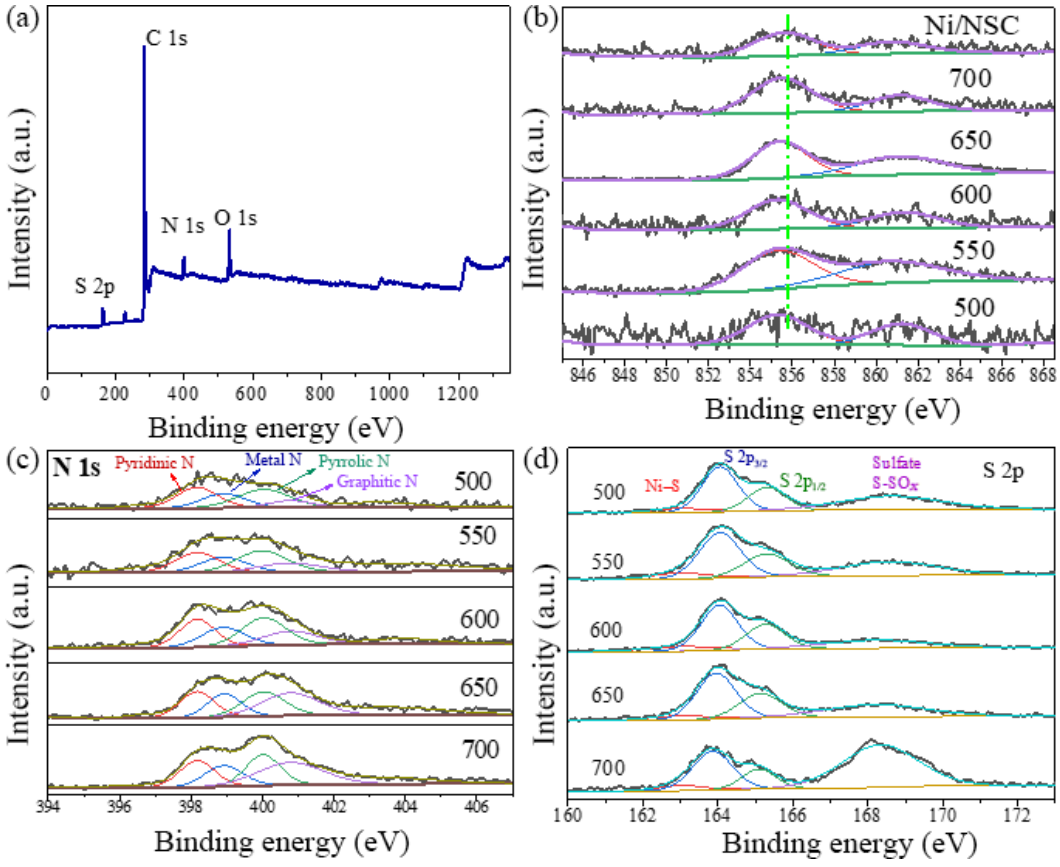

Figure 2 (a) Full spectrum analysis of Ni-NSC-600 catalyst. (b) Ni 2p XPS spectra of Ni/ NSC and Ni-NSC catalysts with different pyrolysis temperature. (c) N 1s and (d) S 2p XPS spectra of Ni-NSC catalysts prepared at different pyrolysis temperatures.

in Ni/C, implying that the binding energy of Ni species in Ni-NSC-600 is between 852 (Ni^0) and 856 eV (Ni^{2+}) [24].

Figure 2(c) shows the high-resolution N 1s spectra of Ni-NSC obtained at different pyrolysis temperatures. The peaks around 398.3, 98.9, 400.0 and 400.8 eV are assigned to the pyridinic N, Ni-N, pyrrolic N, graphitic N, and oxidized N, respectively [25–27]. With the increase of pyrolysis temperature, as shown in Table S2 in the ESM, the content of graphitic N increases from 11.06% to 34.24%, while the content of other N species decreases gradually. However, the content of N element, as shown in Table S1 in the ESM, climbs to the highest after pyrolysis at 600 °C, which is conducive to the anchoring of active Ni component. Besides, it is also found that the S content decreases gradually with the rising pyrolysis temperature. As for the high-resolution S 2p spectra of Ni-NSC, which is shown in Fig. 2(d), the peak around 163.0 eV belongs to the Ni–S, suggesting the coordination of S element with Ni species. While the peaks at 164.0 and 165.3 eV are ascribed to the S $2p_{3/2}$ and S $2p_{1/2}$, respectively, which corresponds to the formation of C–S–C structure. The peak appearing at 168.3 eV is related to the formation of C-SO_x structure [28]. It is found that the peak intensity regarding C-SO_x species decreases gradually when the pyrolysis temperature is raised from 500 to 600 °C, and then increases gradually when the temperature is further elevated to 700 °C. The other peaks like Ni–S, S $2p_{3/2}$, and S $2p_{1/2}$ show the opposite trend. This change also demonstrated that the pyrolysis temperature has effect on not only the content of S but also the type of S species. These above XPS analysis results preliminarily unveil that the dual-doped coordination environment of atomically dispersed Ni species has typical Ni–N and Ni–S bonds. Moreover, the ratio among different Ni species in the chemical state of Ni–N, Ni–S, and Ni determined by XPS and ICP is 3.1:1.0:1.0, suggesting that each Ni atom is coordinated with three N and one S atoms, which is also verified by the following XAS characterizations.

The XAS measurements were performed to further confirm the coordination environment of Ni atom in Ni-NSC-600 catalyst. The Ni K-edge X-ray absorption near-edge spectroscopy (XANES) of Ni-NSC-600 catalyst is showed in Fig. 3(a), with Ni foil, nickel phthalocyanine (NiPc), and NiO as references. It is noted that the XANES of Ni-NSC-600 catalyst is between the spectra of Ni foil and NiO references, indicating that the valence state of Ni species in Ni-NSC-600 catalyst is between the Ni^0 and Ni^{2+} [29, 30]. The Fourier transform (FT) k^2-weighted extended X-ray absorption fine structure (EXAFS) shows that the main peak of Ni-NSC-600 catalyst locates at 1.58 Å, and no characteristic peak of Ni–Ni is observed at 2.1 Å, providing that the Ni species are atomically dispersed on the carbon material. According to the reference samples of NiPc and NiO, as shown in Fig. 3(b), the peaks of Ni–N and Ni–O can be noticed at 1.48 and 1.67 Å, respectively [31]. Then the wavelet transform (WT) was carried out to further analyze the Ni K-edge EXAFS oscillations, as shown in Fig. 3(c) [32, 33]. WT contour plots of Ni foil and NiO exhibit the maximum intensity at 7.0 Å, while the NiPc shows maximum strength at 4.3 Å in the *k*-space. The WT of Ni-NSC-600 only shows one maximum peak at 4.0 Å, which can be attributed to the Ni–N contribution. Therefore, the main peak of Ni-NSC-600 in FT is assigned to Ni–N bond, and the shift of the peak compared with NiPc may be due to the S doping. The quantitative chemical configuration of Ni atom is further proved. To further demonstrate the quantitative chemical

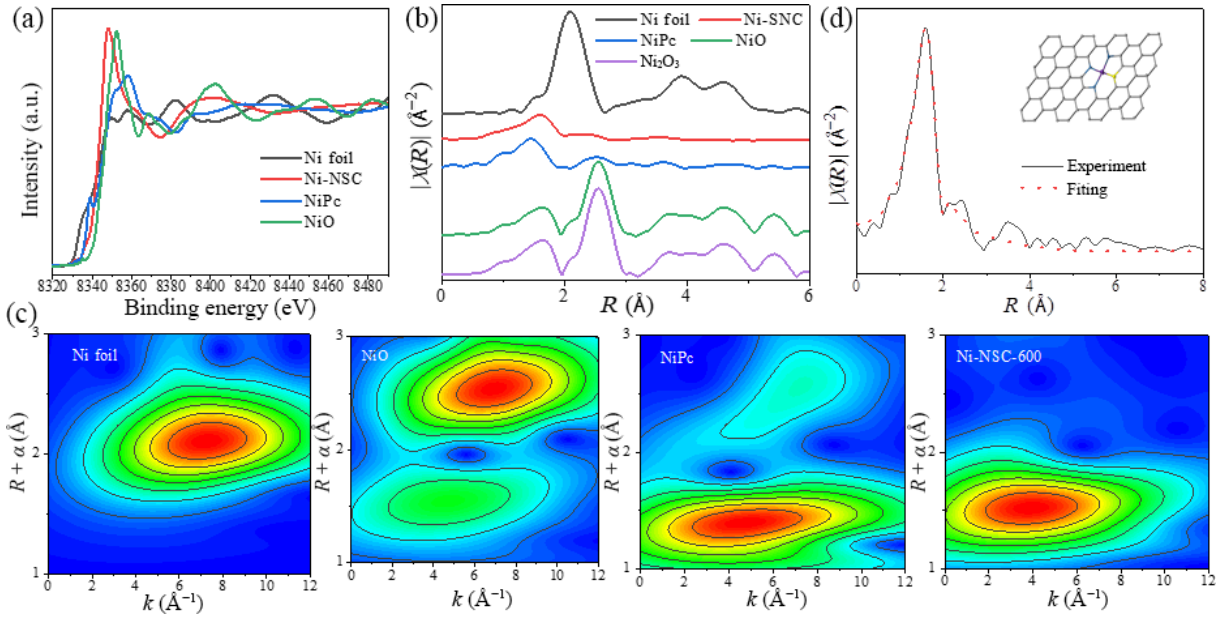

Figure 3 (a) XANES, (b) FT of EXAFS, (c) WT images, and (d) EXAFS fitting result of Ni-NSC-600.

configuration of Ni atom, the EXAFS fitting of Ni-NSC-600 was performed in *R* (Fig. 3(d)) and *k* (Fig. S3 in the ESM) spaces, and the results are consistent with the experimental data [34]. The coverage coordination number of Ni–N is 3.1 at 2.01 Å, and the Ni–S coordination number is 1.2 at 1.90 Å, as shown in Table S3 in the ESM. Combined with the XPS and XAFS characterization results, the coordination environment of Ni component is an asymmetrically isolated Ni-N_3S_1 with four-coordinated moieties, which is constructed in Fig. 3(d).

3.2 Catalytic evaluation

The hydrogenation activity of catalysts with different pyrolysis temperatures is shown in Fig. 4, and the selectivity of MA maintains stably at 100% at our hydrogenation reaction conditions. However, as shown in Fig. 4(a), the Ni-NSC-600 has lower turnover frequency (TOF) of Ni active sites than Ni-NSC-550, but has the highest MP yield rate due to the higher Ni content. Besides, the catalytic performance of Ni/NSC catalyst with the same Ni loading to Ni-NSC-600 was also evaluated under the same reaction conditions. The MP yield rate is only 44.75 mg·g_{cat}^{-1}·h^{-1}, which is much lower than that of Ni-NSC-600 (Fig. 4(b)). Afterwards, the catalytic stability of Ni-NSC-600 and Ni/NSC catalysts was also compared under the same reaction condition, which is displayed in Fig. 5. The Ni-NSC-600 catalyst shows better durability, and the yield rate of MP only shows a slight change after five cycles. However, the activity of Ni/NSC catalyst decreases to 6.63 mg·g_{cat}^{-1}·h^{-1} after only three runs. These results conclude that the Ni-NSC-600 with Ni-N_3S_1 structure presents higher catalytic activity and stability than Ni/NSC. For the used catalyst, as shown in in Fig. S4 and Table S4 in the ESM, the Ni content is 1.27% in Ni-NSC-600-used catalyst after five cycle tests, and there is no obvious agglomeration phenomenon. However, the Ni content is only 0.36% in Ni/NSC-used catalyst after three cycle tests, and there is obvious agglomeration phenomenon, as demonstrated by XRD and HRTEM test.

3.3 Catalytic mechanism

DFT calculations were performed to understand the higher hydrogenation activity of Ni-NSC-600 catalyst than Ni/NSC catalyst. First, the catalyst was prepared and made a further optimization (Fig. S5 in the ESM), then the reaction process was simulated according to the reaction mechanism proposed by Smith (Fig. S6 in the ESM) [35]. Figure 6 shows the adsorption energy of MA and the energy profile for the hydrogenation of MA to *MP on the Ni-NSC and Ni/NSC catalysts. It is noted that the adsorption energy of MA on Ni single-atom is lower than on Ni/NSC catalyst.

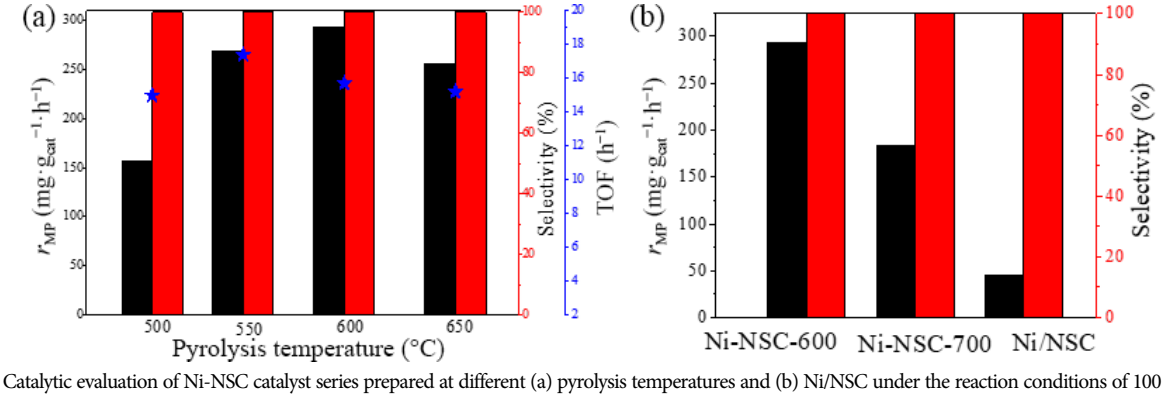

Figure 4 Catalytic evaluation of Ni-NSC catalyst series prepared at different (a) pyrolysis temperatures and (b) Ni/NSC under the reaction conditions of 100 mg catalyst, 500 mg MA, 20 mL solvent, 70 °C, 1 MPa H_2, 300 r·min^{-1}, and 6 h.

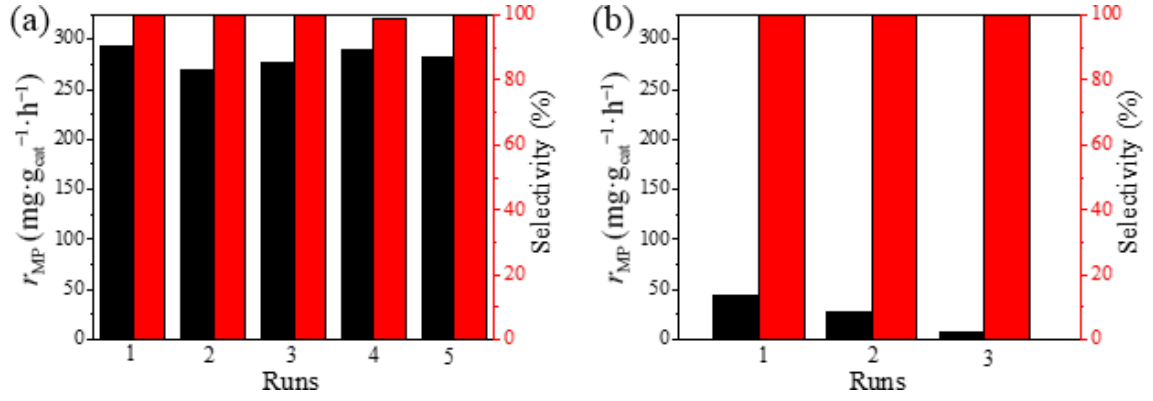

Figure 5 Catalytic stability test for (a) Ni-NSC-600 and (b) Ni/NSC catalysts at the reaction conditions of 100 mg catalyst, 500 mg MA, 20 mL solvent, 70 °C, 1 MPa H_2, 300 r·min^{-1}, and 6 h.

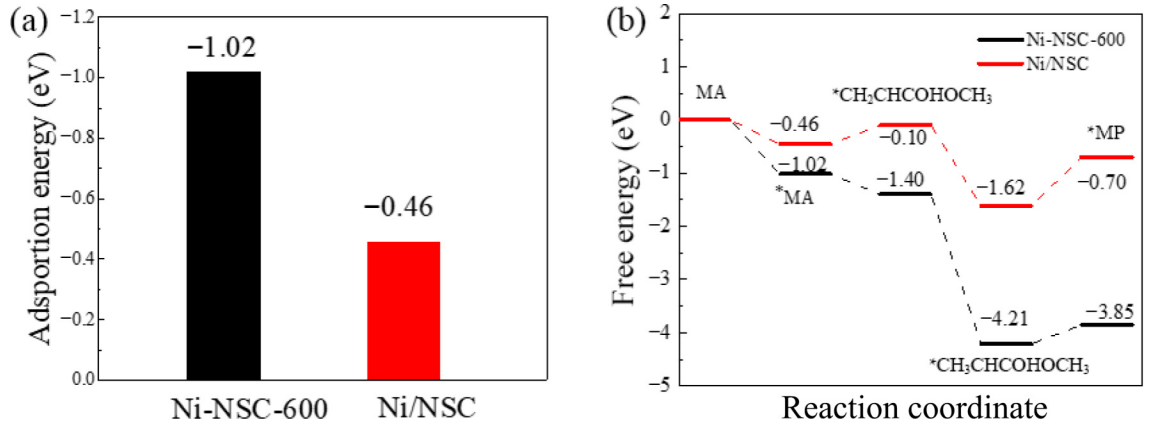

Figure 6 (a) The adsorption energy of MA on the Ni-NSC-600 and Ni/NSC catalysts. (b) Energy profile for the hydrogenation of adsorbed MA to *MP on the Ni-NSC-600 and Ni/NSC catalysts.

Besides, the energy barrier for the transformation of MA to *$CH_2CHCOHOCH_3$, a crucial intermediate during hydrogenation, on Ni-NSC was calculated as −1.40 eV, which is lower than that on Ni/NSC (−0.1 eV). In addition, the Ni-NSC catalyst exhibits a lower adsorption energy for *$CH_3CHCOHOCH_3$ species (−4.21 eV) on Ni-NSC than that on Ni/NSC (−1.62 eV). The DFT calculation results confirmed that the Ni single-atom catalyst with coordination of doped N and S facilitates the formation of *$CH_2CHCOHOCH_3$ and *$CH_3CHCOHOCH_3$ intermediates and desorption of *MP species on catalyst surface. According to these results, it can be believed that the Ni-NSC-600 catalyst is more active than Ni/NSC on the hydrogenation of MA, which is in accordance with the experimental observation.

4 Conclusions

In this study, we successfully developed a Ni single-atom catalyst with the coordination structure of Ni-N_3S_1 by pyrolysis of organic Ni-based precursor. The pyrolysis temperature showed a great influence on the content and the types of N and S elements. With the increase of pyrolysis temperature, the density of N and C–S–C structure shows a volcano tendence and climbs to the peak value at 600 °C, which is conducive to anchor the Ni atom in the catalyst. The Ni single-atom dispersion was confirmed by HAADF-STEM and the Ni-N_3S_1 structure was confirmed by EXAFS analysis. The Ni-NSC-600 catalyst shows the highest catalytic performance, with the yield rate of 293.38 mg·g_{cat}^{-1}·h^{-1} and 100% selectivity of MP at 70 °C and 1 MPa H_2, which are higher than those of Ni/NSC catalyst. The weaker adsorption energy of MA, lower energy barrier of *$CH_2CHCOHOCH_3$ and *$CH_3CHCOHOCH_3$ intermediates on Ni-NSC catalyst promoted the hydrogenation of MA, demonstrating higher catalytic activity of Ni-NSC-600 than Ni/NSC. Besides, the Ni-NSC-600 catalyst displayed excellent durability than Ni/NSC catalyst, which may be contributed to the prevention of Ni aggregation through the strong coordination of Ni atom with N and S.

Electronic Supplementary Material: Supplementary material (the ICP-OES, BET, and XPS analysis for Ni-NSC catalysts with different pyrolysis temperatures, XRD and HRTEM for Ni/NSC catalyst, EXAFS fitting *k* space and EXAFS fittings for Ni-NSC-600, XRD, HRTEM, and ICP-OES results for Ni-NSC-600-used and Ni/NSC catalysts, establishment of catalyst model, and catalytic mechanism of methyl acrylate hydrogenation) is available in the online version of this article at https://doi.org/10.26599/NR.2025.94907053.

Data availability

All data needed to support the conclusions in the paper are presented in the manuscript and the Electronic Supplementary Material. Additional data related to this paper may be requested from the corresponding author upon request.

Acknowledgements

This research was funded by the National Key Research and Development Program of China (Nos. 2023YFA1507800 and 2023YFA1507803), National Natural Science Fund for Distinguished Young Scholars (No. 22025803), and the National Natural Science Foundation of China (No. 22178338).

Declaration of competing interest

All the contributing authors reports no conflict of interests in this work.

Author contribution statement

T. L. S.: Data curation, writing manuscript, experimental design. C. J.: Data curation, validation, experimental design, software. G. W.: Funding acquisition. H. Z.: Review & editing, software. G. L. Z.: Review & editing, supervision. Z. X. L.: Project administration, funding acquisition, conceptualization. C. S. L.: Project administration, funding acquisition. All the authors have approved the final manuscript.

Use of AI statement

None.

References

[1] Chen, Z.; Wu, D. D. Novel route for the synthesis of methyl propionate from 3-pentanone with dimethyl carbonate over solid bases. *Ind. Eng. Chem. Res.* **2011**, *50*, 12343–12348.

[2] Ai, M. Formation of methyl methacrylate from methyl propionate and methanol. *Catal. Today* **2006**, *111*, 398–402.

[3] Wu, D. D.; Chen, Z.; Li, S. D.; Jia, Z. B. Synthesis of methyl propionate from dimethyl carbonate and 3-pentanone over solid base catalyst. *Petrochem. Technol.* **2009**, *38*, 423–427.

[4] Aloui, A.; Delbecq, F.; De Bellefon, C.; Sautet, P. Understanding the influence of hydrogen pressure on the enantioselectivity of hydrogenation: A combined theory–experiment approach. *J. Organomet. Chem.* **2017**, *836–837*, 90–99.

[5] Girvin, Z. C.; Lampkin, P. P.; Liu, X. Y.; Gellman, S. H. Catalytic intramolecular conjugate additions of aldehyde-derived enamines to α,β-unsaturated esters. *Org. Lett.* **2020**, *22*, 4568–4573.

[6] Hong, Z. Studies on catalyzed hydrogenation of olefins by palladium(II) complexes with polyfunctional(P,N,O) phosphine ligands. *J. Mol. Cata.* **2001**, *15*, 451–453.

[7] Toshima, N.; Shiraishi, Y.; Shiotsuki, A.; Ikenaga, D.; Wang, Y. Novel synthesis, structure and catalysis of inverted core/shell structured Pd/Pt bimetallic nanoclusters. *Eur. Phys. J. D* **2001**, *16*, 209–212.

[8] Shiraishi, Y.; Nakayama, M.; Takagi, E.; Tominaga, T.; Toshima, N. Effect of quantity of polymer on catalysis and superstructure size of polymer-protected Pt nanoclusters. *Inorg. Chimi. Acta* **2000**, *300–302*, 964–969.

[9] Matsushita, T.; Shiraishi, Y.; Horiuchi, S.; Toshima, N. Synthesis and catalysis of polymer-protected Pd/Ag/Rh trimetallic nanoparticles with a core–shell structure. *Bull. Chem. Soc. Jpn.* **2007**, *80*, 1217–1225.

[10] van der Zon, M.; Hamersma, P. J.; Poels, E. K.; Bliek, A. Gas–solid adhesion and solid–solid agglomeration of carbon supported catalysts in three phase slurry reactors. *Catal. Today* **1999**, *48*, 131–138.

[11] Chen, C. F.; Sun, J. T.; Li, H.; He, B. L. Studies on the hydrogenation of methyl acrylate catalyzed by Pd/DVB crosslinked poly-(n-vinyl pyrrolidone). *Chin. J. Poly. Sci.* **1990**, *8*, 295–301.

[12] Sun, T. L.; Wu, Z. Y.; Wang, G.; Li, Z. X.; Li, C. S.; Wang, E. Q. Efficient promotional effects of Mo on the catalytic hydrogenation of methyl acrylate over Ni-based catalysts under mild conditions. *Ind. Eng. Chem. Res.* **2022**, *61*, 152–163.

[13] Sun, T. L.; Wang, G.; Guo, X. P.; Li, Z. X.; Wang, E. Q.; Li, C. S. A highly active NiMoAl catalyst prepared by a solvothermal method for the hydrogenation of methyl acrylate. *Catalysts* **2022**, *12*, 1118.

[14] Liu, W. G.; Chen, Y. J.; Qi, H. F.; Zhang, L. L.; Yan, W. S.; Liu, X. Y.; Yang, X. F.; Miao, S.;Wang, W. T.; Liu, C. G. et al. A durable nickel single-atom catalyst for hydrogenation reactions and cellulose valorization under harsh conditions. *Angew. Chem., Int. Ed* **2018**, *57*, 7071–7075.

[15] Dai, X. Y.; Chen, Z.; Yao, T.; Zheng, L. R.; Lin, Y.; Liu, W.; Ju, H. X.; Zhu, J. F.; Hong, X.; Wei, S. Q. et al. Single Ni sites distributed on N-doped carbon for selective hydrogenation of acetylene. *Chem. Commun.* **2017**, *53*, 11568–11571.

[16] Guo, J. Y.; Shang, W. Z.; Hu, J. W.; Xin, C. C.; Cheng, X. S.; Wei, J. Z.; Zhu, C.; Liu, W.; Shi, Y. T. Synergistically enhanced single-atom nickel catalysis for alkaline hydrogen evolution reaction. *ACS Appl. Mater. Interfaces* **2022**, *14*, 29822–29831.

[17] Zhang, J. Q.; Zhao, Y. F.; Chen, C.; Huang, Y. C.; Dong, C. L.; Chen, C. J.; Liu, R. S.; Wang, C. Y.; Yan, K.; Li, Y. D. et al. Tuning the coordination environment in single-atom catalysts to achieve highly efficient oxygen reduction reactions. *J. Am. Chem. Soc.* **2019**, *141*, 20118–20126.

[18] Yuan, Q.; Li, Y. Y.; Yu, P. P.; Ma, B. Y.; Xu, L.; Sun, Q. T.; Yang, H.; Xie, M.; Cheng, T. Reaction mechanism on Ni-C_2-NS single-atom catalysis for the efficient CO_2 reduction reaction. *J. Exp. Nanosci.* **2021**, *16*, 255–264.

[19] Hu, B. T.; Huang, A. J.; Zhang, X. J.; Chen, Z.; Tu, R. Y.; Zhu, W.; Zhuang, Z. B.; Chen, C.; Peng, Q.; Li, Y. D. Atomic Co/Ni dual sites with N/P-coordination as bifunctional oxygen electrocatalyst for rechargeable zinc-air batteries. *Nano Res.* **2021**, *14*, 3482–3488.

[20] Li, Q. H.; Chen, W. X.; Xiao, H.; Gong, Y.; Li, Z.; Zheng, L. R.; Zheng, X. S.; Yan, W. S.; Cheong, W. C.; Shen, R. G. et al. Fe isolated single atoms on S,N codoped carbon by copolymer pyrolysis strategy for highly efficient oxygen reduction reaction. *Adv. Mater.* **2018**, *30*, 1800588.

[21] Qu, M.; Chen, Z.; Sun, Z. Y.; Zhou, D. N.; Xu, W. J.; Tang, H.; Gu, H. F.; Liang, T.; Hu, P. F.; Li, G. W. et al. Rational design of asymmetric atomic Ni-P_1N_3 active sites for promoting electrochemical CO_2 reduction. *Nano Res.* **2023**, *16*, 2170–2176.

[22] Zhao, S. Y.; Cheng, Y.; Veder, J. P.; Johannessen, B.; Saunders, M.; Zhang, L. J.; Liu, C.; Chisholm, M. F.; De Marco, R.; Liu, J. et al. One-pot pyrolysis method to fabricate carbon nanotube supported Ni single-atom catalysts with ultrahigh loading. *ACS Appl. Energy Mater.* **2018**, *1*, 5286–5297.

[23] Cheng, Y.; Zhao, S. Y.; Johannessen, B.; Veder, J. P.; Saunders, M.; Rowles, M. R.; Cheng, M.; Liu, C.; Chisholm, M. F.; De Marco, R. et al. Atomically dispersed transition metals on carbon nanotubes with ultrahigh loading for selective electrochemical carbon dioxide reduction. *Adv. Mater.* **2018**, *30*, 1706287.

[24] Abbas, S. A.; Song, J. T.; Tan, Y. C.; Nam, K. M.; Oh, J.; Jung, K. D. Synthesis of a nickel single-atom catalyst based on Ni-$N_{4-x}C_x$ active sites for highly efficient CO_2 reduction utilizing a gas diffusion electrode. *ACS Appl. Energy Mater.* **2020**, *3*, 8739–8745.

[25] Jin, S.; Ni, Y. X.; Hao, Z. M.; Zhang, K.; Lu, Y.; Yan, Z. H.; Wei, Y. J.; Lu, Y. R.; Chan, T. S.; Chen, J. A universal graphene quantum dot tethering design strategy to synthesize single-atom catalysts. *Angew. Chem., Int. Ed.* **2020**, *59*, 21885–21889.

[26] Li, X. N.; Huang, X.; Xi, S. B.; Miao, S.; Ding, J.; Cai, W. Z.; Liu, S.; Yang, X. L.; Yang, H. B.; Gao, J. J. et al. Single cobalt atoms anchored on porous N-doped graphene with dual reaction sites for efficient fenton-like catalysis. *J. Am. Chem. Soc.* **2018**, *140*, 12469–12475.

[27] Xiong, W. F.; Li, H. F.; Wang, H. M.; Yi, J. D.; You, H. H.; Zhang, S. Y.; Hou, Y.; Cao, M. N.; Zhang, T.; Cao, R. Hollow mesoporous

carbon sphere loaded Ni-N_4 single-atom: Support structure study for CO_2 electrocatalytic reduction catalyst. *Small* **2020**, *16*, 2003943.

[28] Yang, X.; Cheng, J.; Lv, H. K.; Yang, X.; Ding, L. W.; Xu, Y.; Zhang, K.; Sun, W. F.; Zhou, J. H. Sulfur-doped unsaturated Ni-N_3 coordination for efficient electroreduction of CO_2. *Chem. Eng. J.* **2022**, *450*, 137950.

[29] Jeong, H. Y.; Balamurugan, M.; Choutipalli, V. S. K.; Jo, J.; Baik, H.; Subramanian, V.; Kim, M.; Sim, U.; Nam, K. T. Tris(2-benzimidazolylmethyl)amine-directed synthesis of single-atom nickel catalysts for electrochemical CO production from CO_2. *Chem.: Eur. J.* **2018**, *24*, 18444–18454.

[30] Huang, R. K.; Cao, C. Y.; Liu, J.; Zheng, L. R.; Zhang, Q. H.; Gu, L.; Jiang, L.; Song, W. G. Integration of metal single atoms on hierarchical porous nitrogen-doped carbon for highly efficient hydrogenation of large-sized molecules in the pharmaceutical industry. *ACS Appl. Mater. Interfaces* **2020**, *12*, 17651–17658.

[31] Zeng, L. Y.; Liu, Z.; Sun, K. A.; Chen, Y. J.; Zhao, J. C.; Chen, Y. J.; Pan, Y.; Lu, Y. K.; Liu, Y. Q.; Liu, C. G. Multiple modulations of pyrite nickel sulfides via metal heteroatom doping engineering for boosting alkaline and neutral hydrogen evolution. *J. Mater. Chem. A* **2019**, *7*, 25628–25640.

[32] Zhang, Z. T.; Yang, S. M.; Jiang, R.; Sheng, T.; Shi, C. F.; Chen, Y. G.; Wang, L. Y. Intensifying uneven charge distribution via geometric distortion engineering in atomically dispersed M-N_x/S sites for efficient oxygen electroreduction. *Nano Res.* **2022**, *15*, 8928–8935.

[33] Yang, L. P.; Zhang, X.; Yu, L. X.; Hou, J. H.; Zhou, Z.; Lv, R. T. Atomic Fe-N_4/C in flexible carbon fiber membrane as binder-free air cathode for Zn-air batteries with stable cycling over 1000 h. *Adv. Mater.* **2022**, *34*, 2105410.

[34] Fei, H. L.; Dong, J. C.; Arellano-Jiménez, M. J.; Ye, G. L.; Dong Kim, N.; Samuel, E. L. G.; Peng, Z. W.; Zhu, Z.; Qin, F.; Bao, J. M. et al. Atomic cobalt on nitrogen-doped graphene for hydrogen generation. *Nat. Commun.* **2015**, *6*, 8668.

[35] Smith, G. V.; Roth, J. A. Evidence for homolytic mechanism in metal-catalyzed hydrogenation and exchange of α,β-unsaturated esters. *J. Catal.* **1965**, *4*, 406–407.